Determinant Factors of Three-Dimensional Aromaticity in Antiaromatic Cyclophanes

Hiroyuki Kawashima,[†] Shusaku Ukai,[†] Ryo Nozawa,[†] Norihito Fukui,[†] Garrett Fitzsimmons,[§] Tim Kowalczyk,[§]* Heike Fliegl,[‡]* and Hiroshi Shinokubo*,[†]

† Department of Molecular and Macromolecular Chemistry, Graduate School of Engineering, Nagoya University, Furo-cho, Chikusa-ku, Nagoya, Aichi 464-8603, Japan

‡ Karlsruhe Institute of Technology, Institute of Nanotechnology, Hermann-von-Helmholtz-Platz 1, 76344 Eggenstein-Leopold-shafen, Germany

§ Department of Chemistry, Advanced Materials Science & Engineering Center and Institute for Energy Studies, Western Washington University, Bellingham, WA 98229, USA

E-mail: hshino@chembio.nagoya-u.ac.jp; kowalct2@wwu.edu; heike.fliegl@kit.edu

ABSTRACT: Three-dimensional aromaticity arising from the close stacking of two antiaromatic π-conjugated macrocycles has recently received considerable attention. Here, a cyclophane consisting of two antiaromatic Ni(II) norcorrole units tethered with two flexible alkyl chains was synthesized. The norcorrole cyclophane showed crystal polymorphism providing three different solid-state structures. Surprisingly, one of them adopted an aligned face-to-face stacking arrangement with negligible displacement along the slipping axis. Although the exchange repulsion between two π-clouds should be maximized in this orientation, the π–π distance is remarkably close (3.258 Å). Three-dimensional aromaticity in this conformation has been supported experimentally and theoretically as evidenced by small bond length alternation as well as the presence of a diatropic ring current. An analogous cyclophane with two aromatic Ni(II) porphyrin units was prepared for comparison. The porphyrin cyclophane exhibited a slipped-stacking conformation with a larger displacement (2.9 Å) and a larger interplanar distance (3.402 Å) without noticeable change of the aromaticity of each porphyrin unit. In solution, the norcorrole cyclophane forms a twist stacking arrangement with effective interplanar orbital overlap and exists in an equilibrium between stacked and non-stacked structures. Thermodynamic parameters of the stacking process were estimated, revealing an inherently large attractive interaction operating between two norcorrole units, which has been further supported by energy decomposition analysis.

INTRODUCTION

π–π stacking is an essential feature in the crystal engineering of planar π-conjugated molecules because it governs various fundamental physical processes in the condensed phase, namely energy transfer, charge transfer, and phonon transport.[1] Furthermore, π–π stacking significantly contributes to maintaining complex assemblies, i.e. helical structure of DNA and tertiary structure of proteins.[2] In the solid state, π-systems generally favor to form slipped-stacked or staggered arrangements.[3] In contrast, completely overlapped face-to-face stacking is rarely observed because the exchange repulsion between two π-clouds is maximized in this orientation. Exceptional examples include organic π-radicals, where intermolecular exchange interactions are rather attractive due to the presence of unpaired electrons.[4] Consequently, the interplanar distance between two closed-shell π-systems is typically longer than 3.4 Å, which is a sum of the van der Waals radii of two carbon atoms. Considering that the transfer integral between two π-planes should be maximized in the aligned face-to-face arrangement, the creation of this arrangement with a smaller interplanar distance should be beneficial for the future design of practical electronic and optoelectronic materials.

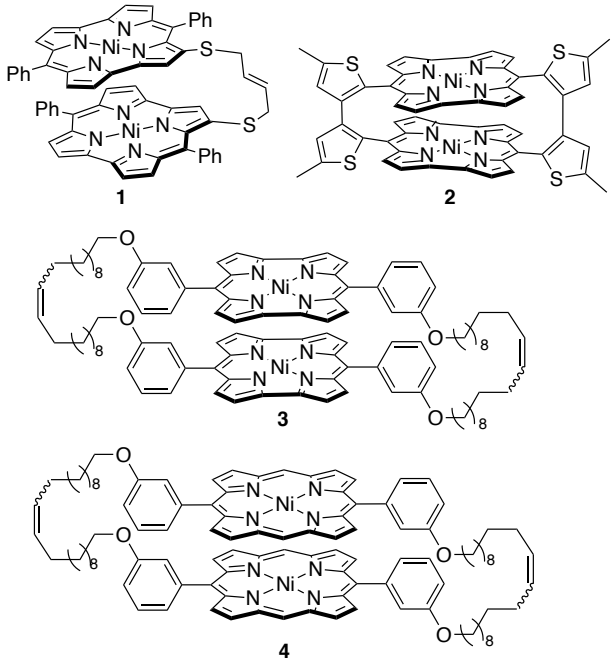

Figure 1. Norcorrole and porphyrin cyclophanes in the present study.

Norcorrole is a ring-contracted porphyrin, which lacks two *meso*-carbon atoms from regular porphyrin.[5,6] Due to 16 π-electrons on its planar π-conjugation pathway, norcorrole Ni(II) complexes exhibit distinct antiaromaticity. Recently, we reported that tethered norcorrole dimer **1** and cyclophane **2** exhibit closely stacked structures with interplanar distances of 3.05 Å (Figure 1).[7] The remarkable proximity of the two norcorrole units has been rationalized by the emergence of three-dimensional aromaticity owing to the spatial delocalization of π-electrons between two antiaromatic systems.[8] However, the two norcorrole units in **1** and **2** still avoided adopting aligned face-to-face stacking, resulting in a twisted arrangement with rotation angles of 66° and 22°, respectively. Furthermore, these previous studies lacked the preparation of the corresponding aromatic counterparts and the investigation into the three-dimensional aromaticity from the energetical point of view.

Here we report the synthesis of norcorrole cyclophane **3**, whose norcorrole units are linked with two flexible alkyl chains (Figure 1). The corresponding porphyrin analogue **4** was also synthesized for comparison. Interestingly, **3** showed crystal polymorphism leading to three different solid-state structures, in which the orientation of the two antiaromatic π-conjugated subsystems is substantially different. The three-dimensional aromaticity in these conformations has been evaluated experimentally and theoretically. The thermodynamic parameters upon the equilibrium between stacked and non-stacked structures in solution were also determined for **3** and **4**.

RESULTS AND DISCUSSION

Synthesis. The synthesis of the target cyclophanes commenced with the preparation of norcorrole and porphyrin Ni(II) complexes **5** and **6** with 3-dodec-11-enyloxyphenyl groups at the *meso*-positions (Scheme 1). The ruthenium-catalyzed olefin metathesis[9] of norcorrole Ni(II) complex **5** under diluted conditions (1.0 mM) afforded norcorrole cyclophane **3** in 26% yield as a mixture of *E* and *Z*-isomers of the internal alkene moiety (*E*,*E*:*E*,*Z*:*Z*,*Z* = ca. 3:3:1). The high-resolution atmospheric pressure chemical ionization (APCI)-TOF mass spectrum of **3** showed a parent ion peak at m/z = 1656.7798 (calcd for $C_{104}H_{116}N_8Ni_2O_4$, m/z = 1656.7821 $[M]^+$), indicating the formation of the macrocyclic dimer. The reaction also furnished macrocyclic norcorrole monomer **7** in 23% yield. The yield of cyclophane **3** was improved to 48% under rather concentrated conditions (2.0 mM). The dilution to 0.5 mM increased the yield of cyclic monomer **7** to 43% yield. Interestingly, the metathesis reaction of porphyrin **6** at 0.1 mM provided only macrocyclic monomer **8** in 57% yield without the formation of target cyclophane **4**. After optimization, cyclophane **4** was obtained in 19% yield under more concentrated conditions at 8.0 mM along with cyclic and acyclic oligomeric porphyrins.

Scheme 1. Synthesis of Norcorrole and Porphyrin Cyclophanes 3 and 4 through Olefin-Metathesis

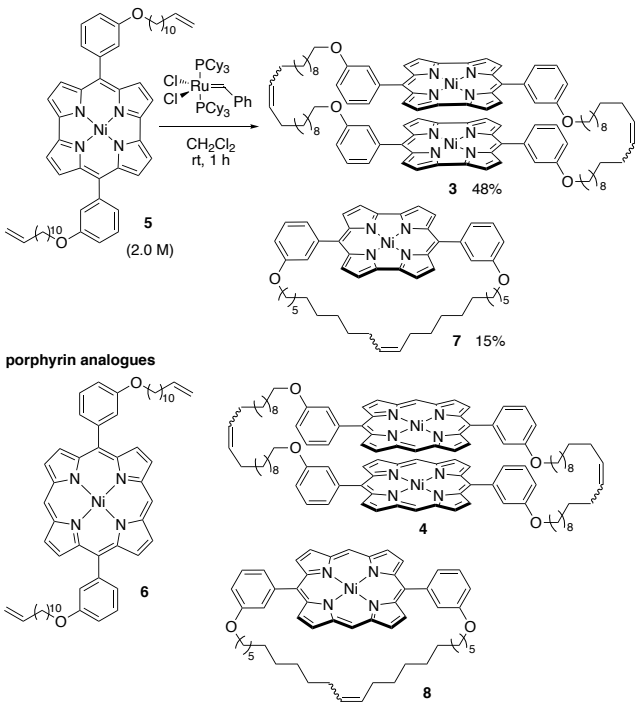

Solid-state structures. We found three crystal polymorphs of norcorrole cyclophane **3** (**α**, **β**, and **γ**) even from the same solvent combination, $CHCl_3$/MeOH (Figures 2–4 and Table S1). In all cases, the two norcorrole planes formed a π–π stacking structure. The observed stacking structures are labeled **A**, **B**, and **C**, corresponding to the polymorphs **α**, **β**, and **γ** respectively.

Slow vapor diffusion of methanol into a chloroform solution of **3** afforded suitable crystals (polymorph **α**) for X-ray diffraction analysis. The norcorrole π-system is slightly distorted to a shallow bowl conformation with a mean plane deviation of 0.082 Å (Figure 2). Importantly, the torsion angle of C_{meso}–Ni–Ni'–C'_{meso} is 0° (Figure 2d). The relative displacement of the Ni(II) centers is ca. 0.5 Å. These results indicate that the two stacking norcorrole cores are almost overlapped. Such aligned face-to-face stacking is counterintuitive in terms of the expected strong exchange repulsion between π-electrons. The distance between the two mean planes of the macrocycles is 3.26 Å, while the distance between the two nickel centers is 2.878 Å. The alkyl substituents adopt a hairpin-like conformation due to the van der Waals interaction.

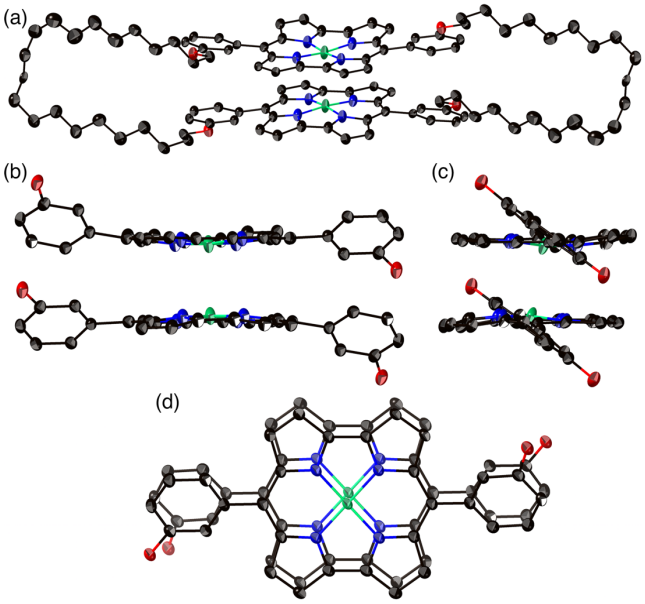

Figure 2. X-ray structure of norcorrole cyclophane **3** (polymorph **α**). (a) Molecular structure. (b–d) Stacking structure of two norcorrole units. Hydrogen atoms and alkyl chains in (b–d) are omitted for clarity.

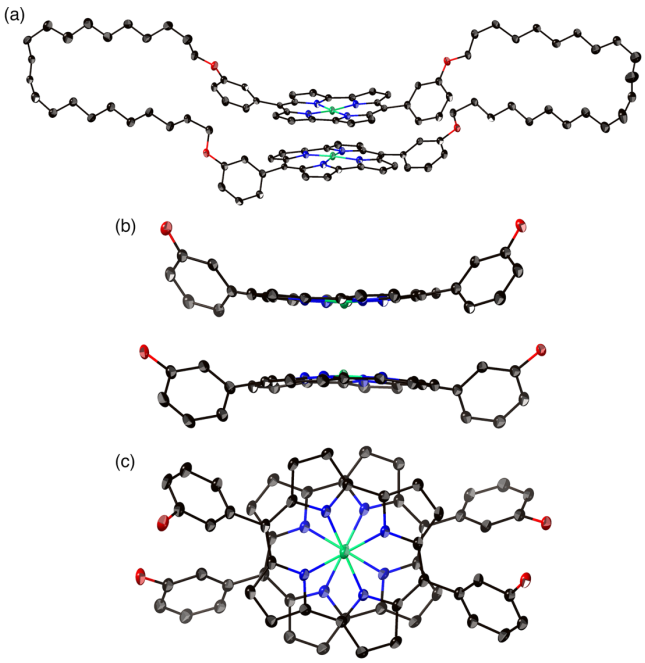

Figure 3. X-ray structure of norcorrole cyclophane **3** (polymorph **β**). (a) Molecular structure. (b, c) Stacking structure of two norcorrole units. Hydrogen atoms and alkyl chains in (b, c) are omitted for clarity.

In polymorph **β**, two norcorrole units again adopt a closely stacked arrangement with an interplanar distance of 3.33 Å (Figure 3). The two π-planes are twisted with a C_{meso}–Ni–Ni'–C'_{meso} dihedral angle of 36°, in which two nickel atoms are located along the rotation axis with a Ni–Ni' distance of 2.934 Å. The orientation of the two norcorroles is similar to the previously reported dinorcorroles **1** and **2**, in which the two macrocycles adopt a twisted conformation.

Polymorph **γ** was obtained by vapor diffusion of methanol into a relatively diluted solution of **3** in chloroform (Figure 4). The resulting π-stacked structure **C** exhibits typical slipped stacking with an interplanar distance of 3.39 Å. The relative displacement of the two macrocycles' centers is 1.5 Å, which is substantially larger than that of **A** and **B**. The distance between the two Ni(II) centers is 3.719 Å. These structural parameters suggest that the interplanar interaction between norcorrole units of **C** is weaker than that of **A** and **B**. The alkyl tethers of **C** are densely packed in comparison to those of **A** and **B**, implying that this conformation is dominated by the van der Waals force between alkyl groups rather than by the interactions between the two macrocycles. Currently, we speculate that the polymorphs of norcorrole cyclophane **3** result from balancing the interaction between the norcorrole macrocycles and the zipper effect among the alkyl linkers.

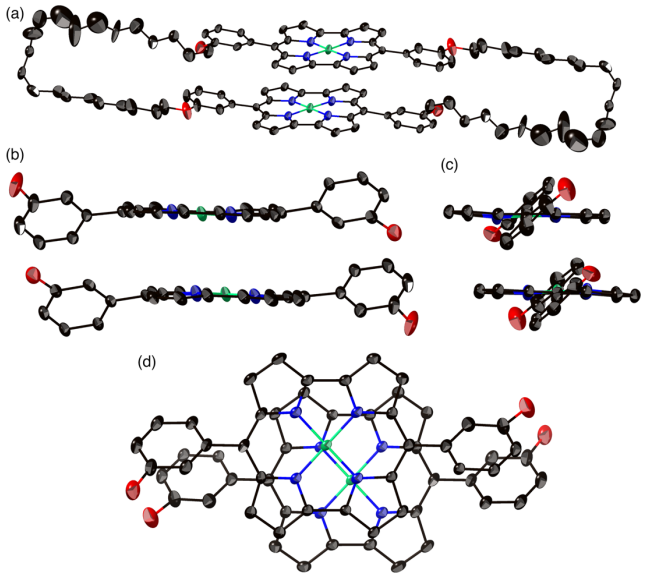

Figure 4. X-ray structure of norcorrole cyclophane **3** (polymorph **γ**). (a) Molecular structure. (b–d) Stacking structure of two norcorrole units. Hydrogen atoms and alkyl chains in (b–d) are omitted for clarity.

The crystal structure of porphyrin cyclophane **4** was also unambiguously elucidated (Figure 5). In sharp contrast to norcorrole cyclophane **3**, the two porphyrin macrocycles adopt a slipped-stacking structure, which is typical for aromatic π-systems. The relative displacement and interplanar distance of the two porphyrin units are 2.9 Å and 3.402 Å, respectively. The interplanar distance is substantially longer than the distances observed in **A** and **B**. The porphyrin framework is distorted with a mean plane deviation of 0.195 Å, which is due to the small ionic radius of Ni(II). The two Ni(II) centers are separated by a distance of 4.462 Å.

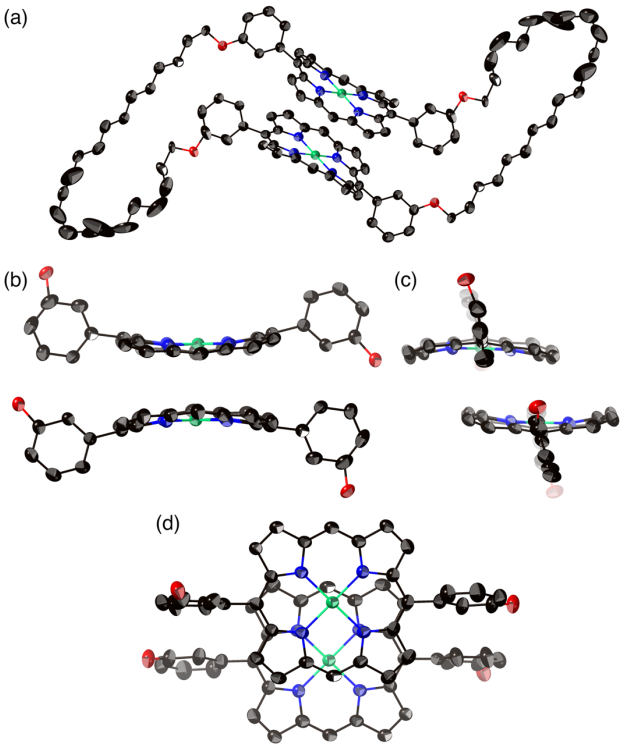

Figure 5. X-ray structure of porphyrin cyclophane **4**. (a) Molecular structure, (b–d) stacking structure of two porphyrin units. Hydrogen atoms and alkyl chains in (b–d) are omitted for clarity.

The bond length alternation (BLA) in cyclic conjugation systems is a good index for the degree of π-electron delocalization in macrocycles. We evaluated BLA on the basis of the harmonic oscillator model of aromaticity (HOMA)[10] analysis (Table 1). The HOMA value in **A** is 0.69, which is larger than those of norcorrole monomer (0.45) and previously reported stacked norcorrole dimers (**1**: 0.55–0.57, **2**: 0.56–0.59). It is noteworthy that the magnitude of the bond length equalization is comparable to that in the aromatic macrocycles in porphyrin cyclophane **4** (HOMA = 0.77). These results indicate that the double bonds in **A** are delocalized in the norcorrole units. In contrast, the HOMA values in **B** (0.41–0.47) and **C** (0.38) are substantially lowered to reveal their less-effective π-electron delocalization. It is also worth noting that the HOMA value of porphyrin cyclophane **4** is comparable to that of 5,10,15,20-tetramesitylporphyrin Ni(II) (0.77),[7a] which means that the change of HOMA values in the stacked conformation has not been observed for the aromatic porphyrin system.

Table 1. HOMA values of norcorrole and porphyrin units in cyclophanes 3 and 4.

structures	HOMA
A	0.69
B	0.41, 0.47
C	0.38
4	0.77
1	0.55, 0.57
2	0.56, 0.59

Ring current effect. The aromaticity/antiaromaticity of norcorrole cyclophanes **3** corresponding to the three polymorph structures (**A**, **B**, and **C**) was evaluated by theoretical calculations on the basis of magnetic criteria by means of nucleus-independent chemical shift (NICS)[11] analyses as well as current density analyses with the gauge-including magnetically induced current (GIMIC) method[12] and anisotropy of the induced current density (ACID) method.[13] The magnetic property of porphyrin cyclophane **4** was also investigated for comparison.

The NICS values of **A**, **B**, and **C** in their crystal structures were calculated at the GIAO-BHLYP/def2-TZVP level, because the B3LYP functional has been reported to overestimate paratropic current strengths.[14] The alkoxy tethers were replaced with hydrogen atoms to reduce the calculation cost. To probe the magnetic effect in both inner and outer spaces of cyclophanes, NICS(1) and NICS(−1) were examined at eight positions 1.0 Å above and below the five-membered and six-membered ring substructures of the norcorrole and porphyrin macrocycles (Table 2 and Figure S29). Importantly, largely negative NICS(1) and NICS(−1) values from −18.0 to −32.5 ppm were provided for **A**, supporting the distinct magnetic aromaticity. On the other hand, the NICS(1) and NICS(−1) values of **C** (27.9–44.1 ppm) are essentially the same as those of the monomeric Ni(II) norcorrole (30.1–36.1 ppm), indicating each norcorrole unit maintains its distinct antiaromaticity. In structure **B**, the NICS(1) and NICS(−1) values (22.2–27.2 ppm) are substantially decreased in comparison to those of **C**, indicating its attenuated antiaromaticity. Furthermore, we optimized several face-to-face stacking arrangements of norcorroles with fixing the twist angles to calculate their NICS values (Figure S32). The results support that the NICS values are highly dependent on the twist angle. In the case of porphyrin cyclophane **4**, the NICS values of the porphyrin units are comparable to those of a monomeric porphyrin.

Table 2. NICS(1) and NICS(−1) values of norcorrole and porphyrin units in cyclophanes 3 and 4.[a]

structures	NICS(1)	NICS(−1)
A	−19.0, −18.3, −18.2, −18.0	−32.5, −30.3, −29.6, −29.1
B	24.1, 23.6, 22.8, 22.2	27.2, 24.5, 23.2, 22.9
C	34.0, 33.1, 32.7, 27.9	44.1, 38.5, 31.1, 30.6
norcorrole monomer	36.1, 35.7, 34.3, 33.7	33.4, 32.4, 31.0, 30.1
4	−23,0, −19.9, −19.2, −19.0	−24.7, −23.4, −23.0, −17.2
porphyrin monomer	−19.6, −19.5, −17.6, −17.5	−19.9, −19.8, −18.4, −18.0

[a] The calculations were conducted at the GIAO-BHLYP/def2-TZVP level.

The two-dimensional NICS plots of three conformations (**A**, **B**, and **C**) of norcorrole cyclophane **3** as well as porphyrin cyclophane **4** are shown in Figure 6. The inspection plane was set between two macrocycles. In structure **A**, the shielded region (ca. −30 ppm) in blue was confirmed in the space surrounded by two norcorrole units, supporting the aromatic nature of cyclophane **3** in the aligned π-stacking orientation (Figure 6a). In contrast, the deshielded region in red exists in the inner space of **B** and **C**, while the magnitude of the deshielding effect in **B** is weaker than that in **C** (Figure 6b and 6c). It is noteworthy that the magnetic shielding effect in **A** is rather stronger than that in aromatic porphyrin cyclophane **4** (Figure 6d).

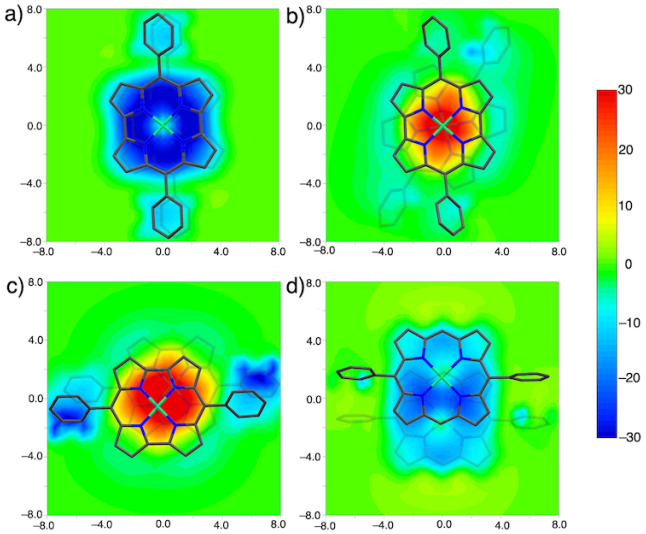

Figure 6. NICS plots of cyclophanes **3** and **4**. a) **A**, b) **B**, c) **C**, and d) **4**. The geometries of cyclophanes were obtained from their crystal structures but the alkoxy tethers were placed with hydrogen atoms to reduce the calculation cost. The calculations were conducted at the GIAO-BHLYP/def2-TZVP level.

The magnetically induced ring currents in different conformations of norcorrole cyclophane **3** were visualized and quantified by a current density analysis with the GIMIC method (Figure 7).[12] In this calculation, the substituents were replaced with hydrogen atoms to simplify the analysis. Figure 7a and 7b demonstrate integrated current strength susceptibilities (in nA T^{-1}) for the antiaromatic norcorrole monomer and aligned stacked dimer **A**, which have net currents of –45.5 and 22.2 nA T^{-1}, respectively. For comparison, the aromatic Ni(II) porphyrin cyclophane **4** has a net current of 28.1 nA T^{-1} at the same level of theory. The clockwise ring current in **A** strongly supports its distinct aromatic nature in magnetic criteria (Movie S1). The ring current is split into two streams at each pyrrolic ring. In the case of the Ni(II) monomer, the current flows preferentially through the inner pathway, while the division of the stream is almost equal in the case of aromatic norcorrole cyclophane **A**. In contrast to cyclophane **A**, the ring current streams in the case of **B** were complicated on the norcorrole macrocycles (Movie S3). Interestingly, **B** exhibited the current stream through the space between two norcorrole units, while such three-dimensional current was not detected in the case of **A** (Movie S2 and S4). The visualized streamlines in **A** lacked in the space current (Figure 7c). On the other hand, three dimensional streamlines in **B** demonstrates the presence of very rich current density interactions. Norcorrole cyclophane **C** clearly shows the counter-clockwise ring current of –49.2 nA T^{-1} due to its distinct antiaromaticity of the norcorrole unit (Figure S38 and Movie S5) without generation of the space current (Movie S6). The ACID plots also confirmed that only **B** showed the inter-norcorrole current stream (Figure S31). The exact reason for existence of the spatial current stream in **B** but not in **A** is currently unclear. We presume that the symmetry difference between **A** and **B** is important. The paratropic contribution of the ring current of antiaromatic porphyrinoids is related to the magnetic dipole transition in the first excited state.[14a] Due to the higher symmetry of **A**, the magnetic dipole transition to the first excited state is parity-forbidden, while **B** exhibits the magnetic dipole allowed transition, which is probably related to the inter-norcorrole current.

The aforementioned calculations clearly conclude the π-stacking distance and the twist angle between two norcorrole units are a crucial determinant for the generation of the three-dimensional aromaticity. Namely, an aligned face-to-face stacking with a short π–π distance is crucial to generate a distinct diatropic ring current.

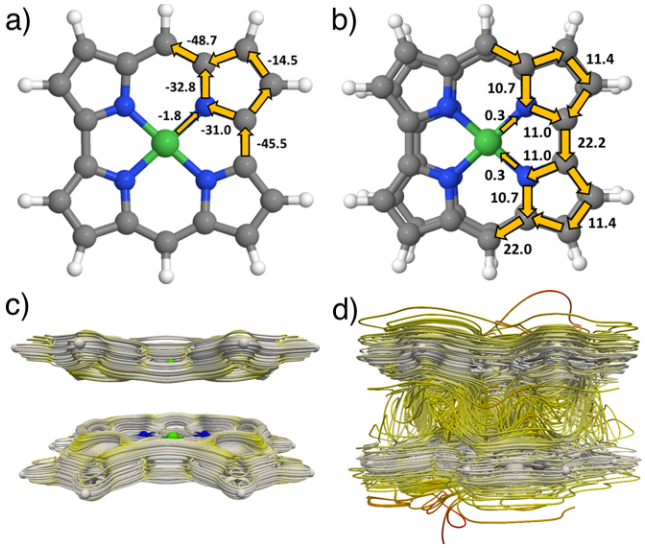

Figure 7. GIMIC analysis of a) norcorrole monomer and b) cyclophane **A** conducted at the GIAO-BHLYP/def2-TZVP level. Integrated current strength susceptibilities across selected bonds are given in nA T^{-1}. The yellow arrows indicate the direction of the current flow. Illustration of the calculated three-dimensional current density represented as three dimensional streamlines in c) cyclophane **A**) and d) cyclophane **B**.

Molecular orbital interactions in norcorrole cyclophane.

To evaluate the orbital interactions, frontier orbitals of norcorrole cyclophanes in three different conformations were examined with the DFT calculations at the B3LYP/def2-TZVP level. As illustrated in Figure 8 and Figure S33, in-phase and out-phase combinations of two HOMOs generate stabilized and destabilized MOs. The aligned orientation of two antiaromatic norcorrole units in **A** maximizes the interaction between HOMOs and LUMOs of two norcorrole macrocycles, which highlights the effective orbital overlap.

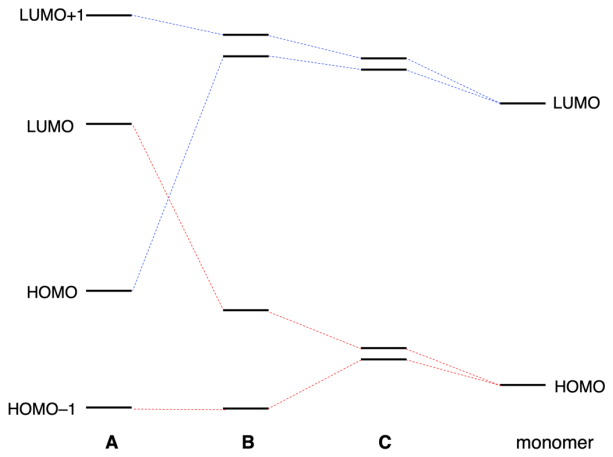

Figure 8. Molecular orbital energy diagrams of norcorrole cyclophane **3**. The geometries of **3** were obtained from their crystal structures but the alkoxy tethers were placed with hydrogen atoms to reduce the

calculation cost. The calculations were conducted at the B3LYP/def2-TZVP level.

Table 3. Transfer integrals for norcorrole cyclophane 3. Calculations were conducted at the B3LYP/def2-TZVP level.[a]

	t_1 [meV] HOMO–HOMO	t_2 [meV] LUMO–LUMO
A	728	745
B	271	34.5
C	42.7	23.3

[a] The geometries of **3** were obtained from their crystal structures but the alkoxy tethers were placed with hydrogen atoms to reduce the calculation cost. The calculations were conducted at the B3LYP/def2-TZVP level.

We estimated the orbital interactions between two norcorroles in **A**, **B**, and **C** in terms of transfer integrals t_1 and t_2 between their individual HOMOs and LUMOs, respectively (Table 3). The values of the transfer integrals were calculated with the corresponding dimer structures in the crystal packing of **A**, **B**, and **C** with the B3LYP/def2-TZVP level using CATNIP.[15] The transfer integrals t_1 and t_2 of **A** are significantly large (728 and 745 meV), supporting effective orbital interactions in both HOMOs and LUMOs in the aligned stacking structure. Because of the large orbital interactions, the combination of LUMOs and HOMOs of the monomer affords HOMO and LUMO of the dimeric cyclophane. The transfer integral t_1 is substantially larger than t_2, indicating the less-effective overlap of the LUMOs in **B**. In **C**, both transfer integrals t_1 and t_2 are moderate due to its well-separated orientation of two π-systems. Naturally, the magnitude of transfer integrals is in line with the splitting of HOMO and LUMO levels in the MO diagrams (Figure 8).

Stacking behaviors of norcorrole and porphyrin cyclophanes in solution. We then explored the stacking dynamics of norcorrole cyclophanes **3** in solution. The ^{1}H NMR spectra of **3** were measured in toluene-d_8 and $CDCl_3$ at various temperatures (Figure S23). The ^{1}H NMR spectrum of **3** in toluene-d_8 at 373 K displayed its pyrrole protons from 2.4 to 3.1 ppm. These signals appeared in the region comparable to those of monomer **7** (1.8–2.4 ppm), indicating that **3** predominantly exists in a non-stacked conformation in solution at this temperature. Cooling of the solution induced apparent down-field shift of these signals, reaching 4.5–5.5 ppm at 193 K. A similar temperature-dependence was also detected in $CDCl_3$. The observed down-field shift is characteristic of stacked norcorrole dimers **1** and **2**,[7] thus suggesting the existence of equilibrium between non-stacked and stacked states. On the basis of nonlinear curve regression analysis of the chemical shift changes (Figure S26), we estimated enthalpy and entropy changes ΔH of –23 kJ mol^{-1} and ΔS of –68 J K^{-1} mol^{-1}, respectively, in toluene-d_8 as well as ΔH of –22 kJ mol^{-1} and ΔS of –59 J K^{-1} mol^{-1} in $CDCl_3$ (Table 4).[16] These values afford association constants at 293 K (K_{293}) of 5.6 and 3.7 in $CDCl_3$ and toluene-d_8, respectively, indicating that ca. 78–85% of **3** adopt a stacked form at room temperature (293 K). The fitting analysis also estimated that pyrrolic proton signals in the stacked form would appear around 4.2–4.6 ppm.

DFT calculations at the BLYP-D3/6-31G(d)+SDD//B97D3/6-31G(d)+SDD level indicate that the energy difference between an aligned stacking structure **A** and a twist stacking structure **B** is almost negligible (0.5 kcal mol^{-1}). The DFT calculation did not reproduce the slipped stacking arrangement in structure **C**. To determine the plausible stacking structure of **3** in solution, we simulated the ^{1}H NMR chemical shifts of structures **A** and **B** by the GIAO calculations at the BHLYP/6-31G(d)//B97D3/6-31G(d)+SDD level of theory (Figure S36 and S37). The solvent effect of chloroform was considered by the PCM model. The calculated chemical shift values of pyrrole protons range from 7.6 to 8.6 ppm for **A** and 4.3–5.4 ppm for **B**. These results suggest that a twisted structure **B** should be dominant in solution.

Because **3** is a mixture of *E*- and *Z*-isomers of the linkers, the ^{1}H NMR spectra contained many signals. Furthermore, the range of temperatures for the curve fitting is limited (263–383 K) due to broadening and splitting of signals. Consequently, we only estimated thermodynamic parameters ΔH and ΔS roughly. To obtain more accurate data, the alkene moieties of **3** were hydrogenated by the aid of Crabtree catalyst to afford **9** in 22% yield (Scheme 2).[17] The ^{1}H NMR spectra of **9** were measured in toluene-d_8 and $CDCl_3$ at various temperatures (Figure 9 and Figure S25). The nonlinear curve regression analysis of the chemical shift changes of the pyrrole protons (temperature range: 213–373 K for toluene-d_8 and 273–333 K for $CDCl_3$) provided ΔH of –17 kJ mol^{-1} and ΔS of –56 J K^{-1} mol^{-1} in toluene-d_8 as well as ΔH of –19 kJ mol^{-1} and ΔS of –57 J K^{-1} mol^{-1} in $CDCl_3$ (Table 4 and Figures 10, S28). These values accord with those of **3**, thus suggesting that the presence of *E*- and *Z*-isomers in **3** does not cause significant errors in evaluation of thermodynamic parameters.

Scheme 2. Hydrogenation of 3.

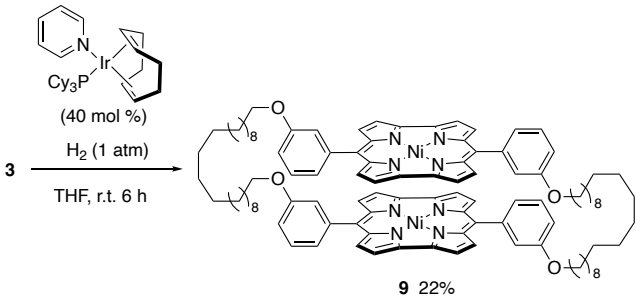

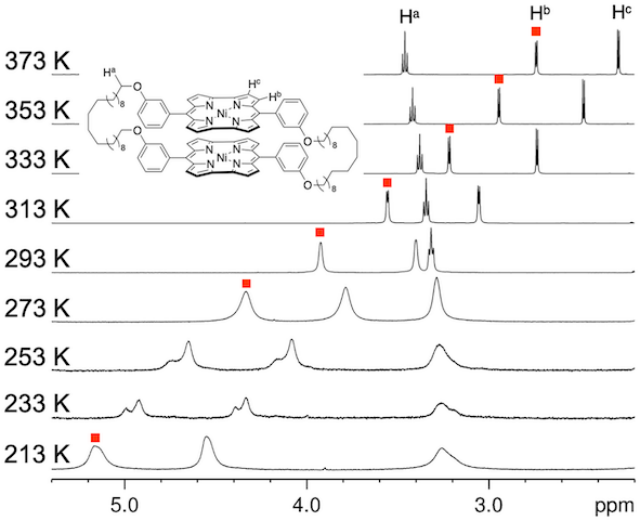

Figure 9. Temperature-dependent ^{1}H NMR spectra of **9** in toluene-d_8. The red squares represent the peaks used for the nonlinear curve regression analysis.

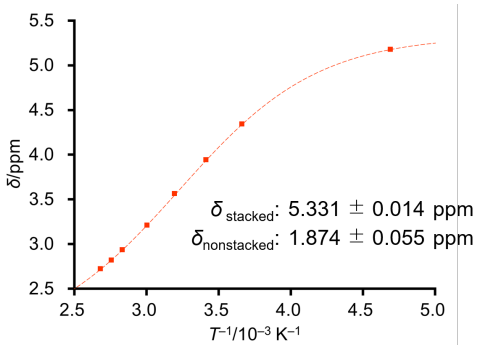

Figure 10. ^{1}H NMR chemical shifts of **9** in toluene-d_8 plotted as a function of temperature. Filled markers represent experimental points. Dash curves correspond to chemical shift calculated from the van't Hoff equation.

Figure 11 shows the UV/vis/NIR absorption spectra of norcorrole cyclophane **3** and its monomer precursor **5**. Monomer **5** shows weak and broad absorption tailing to 1000 nm, which is a characteristic feature of non-aggregated norcorrole Ni(II) complexes. On the other hand, the absorption spectrum of **3** in CH_2Cl_2 at 293 K exhibits a relatively sharp band around 800 nm, which is not present in the spectrum of monomer **5**. This absorption band became intensified upon cooling. The spectral feature of **3** is diagnostic for closely stacked norcorrole dimers **1** and **2**. The TD-DFT calculations for conformer **B** reproduced the experimental absorption spectrum (Figure S34).

To compare the thermodynamic parameters of **3** with those of **4**, the temperature-dependent ^{1}H NMR spectra of porphyrin cyclophane **4** were also measured in toluene-d_8 and $CDCl_3$ (Figure S24). Cooling of the solution of **4** resulted in up-field shifts of the signals due to the *meso*- and pyrrole-protons with the maximum displacement of ca. 0.5 ppm. Similar trends are often observed for the π-stacking of aromatic π-systems, which are attributed to the ring current effect in the cyclic π-system.[18] Curve regression analysis afforded ΔH of –12 kJ mol^{-1} and ΔS of –48 J K^{-1} mol^{-1} in toluene-d_8 as well as ΔH of –15 kJ mol^{-1} and ΔS of –75 J K^{-1} mol^{-1} in $CDCl_3$ (Table 4 and Figure S27). These values afford association constants K_{293} of 0.38 and 0.05 in toluene-d_8 and $CDCl_3$, respectively. The absorption spectrum of porphyrin cyclophane **4** at 298 K exhibits the Soret band at 400 nm, which was blue-shifted to 393 nm upon cooling to 183 K (Figure 12), while porphyrin monomer **6** shows its Soret band at 401 nm. The blue-shifted Soret band of **4** suggests the formation of a H-type aggregate, which accords with the crystal structure. This assumption has also been supported by the TD-DFT calculations at the CAM-B3LYP/6-31G(d)+SDD level of theory (Figure S35).

Table 4. Thermodynamic parameters for equilibrium between non-stacked and stacked conformations.

	solvent	ΔH [kJ mol^{-1}]	ΔS [J K^{-1} mol^{-1}]	K_{293}
3[a]	toluene-d_8	–23	–68	3.7
3[a]	$CDCl_3$	–22	–59	5.6
4[a]	toluene-d_8	–12	–48	0.38
4[a]	$CDCl_3$	–15	–75	0.05
9	toluene-d_8	–17	–56	1.5
9	$CDCl_3$	–19	–57	2.4

[a] Because of the presence of isomers, these parameters were roughly estimated.

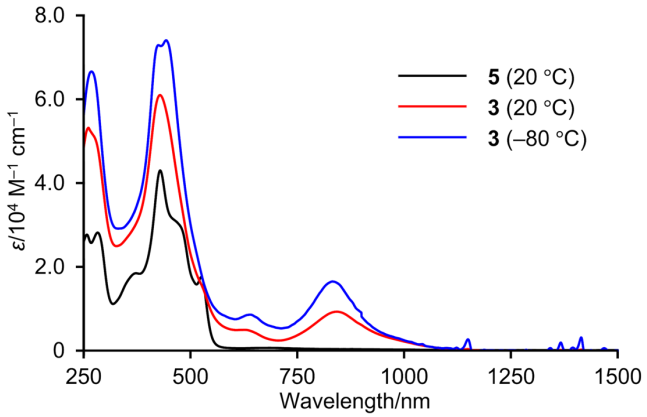

Figure 11. UV/vis absorption spectra of norcorrole cyclophane **3** and monomer **5** in dichloromethane.

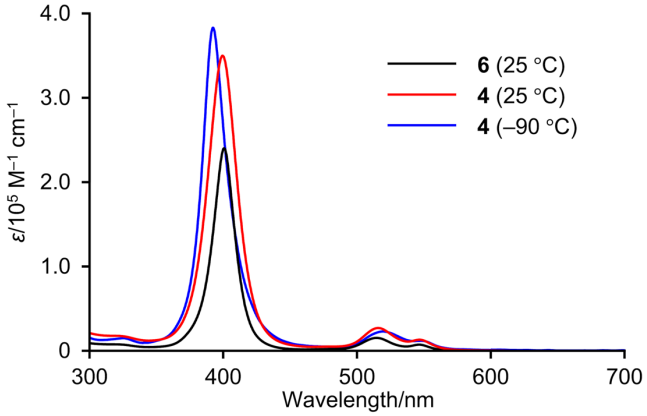

Figure 12. UV/vis absorption spectra of porphyrin cyclophane **4** and monomer **6** in dichloromethane.

The aforementioned studies indicate that stabilization energy associated with the π-stacking of norcorrole is larger than or at least comparable to that of porphyrin. It should be commented that the stacking structures of **3** and **4** are substantially different: norcorrole cyclophane **3** exhibits shorter stacking distance and larger overlapping area between two π-planes. Consequently, **3** should inherently experience more significant enthalpic penalty than **4** due to the severe exchange repulsion in the closely stacking orientation. Nevertheless, norcorrole cyclophane **3** demonstrates clear tendency to adopt the stacked structure. On the basis of these considerations, we concluded that an inherently large attractive interaction is operating between two norcorrole units in **3**. These assumptions have been supported by the following energy decomposition analysis.

Energy decomposition analysis.

The formation and stabilization of different observed polymorphic forms for cyclophane **3** depend on complex electronic interactions between the norcorrole units. To understand the roles of different intermolecular interactions on the internal stabilization of the cyclophane, we performed DFT-based energy decomposition analyses (EDA) of the interacting norcorrole units of structures **A**, **B**, and **C** as well as the porphyrin cyclophane **4** at the ωB97X-D/6-31G(d) level in Q-Chem.[19] EDA quantitatively decomposes the total interaction energy of a dimer into chemically meaningful components including frozen, polarization, dispersion, and charge transfer

interaction energy. For this analysis, the alkoxy tethers were replaced with hydrogens in each crystal structure to reduce computational cost while ensuring an unambiguous separation of the cyclophane into interacting monomers, which is a requirement of the EDA.

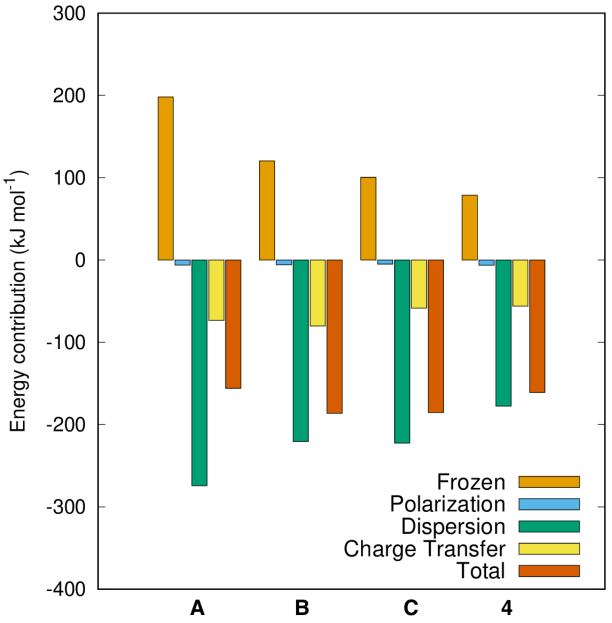

Figure 13. Decomposition of the cyclophane interaction energies into polarization, dispersion, and charge transfer contributions at the ωB97X-D/6-31G(d) level.

The EDA results, summarized in Figure 13, show that dispersion dominates the interaction between the two π-systems in all four structures. Among three structures of norcorrole cyclophane **3**, structure **B** is the most favorable by a small margin, which is in line with experimental observation in solution. The dispersion interaction is stronger for all polymorphs of the stacked norcorroles than for porphyrin analog **4**. The aligned stacking and short interplanar distances in **A** are consistent with its especially strong dispersion interaction, $|E_{disp}(\mathbf{A})| > |E_{disp}(\mathbf{B})| \approx |E_{disp}(\mathbf{C})| > |E_{disp}(\mathbf{4})|$. It should be also noted that **A** and **B** experience stronger repulsive interactions (frozen) than the slipped conformations in **C** and **4** because of the short stacking distances. The strong exchange repulsion is overridden by the strong dispersion interaction in structure **A**. Interestingly, structures **A** and **B** present a similar degree of charge-transfer contribution to the interaction energy despite the difference in the relative orientations of their two norcorrole units. In contrast, the slip-stacking norcorrole polymorph, structure **C**, presents a weaker contribution from charge-transfer interactions that more closely resembles that of **4**, which is also slip-stacked: $|E_{CT}(\mathbf{A})| \approx |E_{CT}(\mathbf{B})| > |E_{CT}(\mathbf{C})| \approx |E_{CT}(\mathbf{4})|$. These considerations based on EDA suggest that there are several ways to stabilize the different stacking structures of two norcorrole units that appear to be energetically similar, supporting the observed polymorphism of **3**. In addition, the zipper effect among the alkyl tethers, which is not evaluated by the present EDA, should also be considered as a contributing factor for the specific stacking orientation.

Mixed-valence states of norcorrole cyclophane 3. The redox behaviors of norcorrole cyclophane **3**, porphyrin cyclophane **4**, norcorrole monomer **5**, and porphyrin monomer **6** were studied by cyclic voltammetry (Figure 14). The cyclic voltammograms were obtained under the following conditions: solvent: CH_2Cl_2; supporting electrolyte: 0.1 M $[Bu_4N][PF_6]$; reference electrode: $Ag/AgNO_3$; scan rate: 0.03 V s^{-1}; external reference: ferrocene.

Norcorrole monomer **5** exhibited reversible oxidation waves at –0.05, 0.27, and 0.83 V as well as reversible reduction waves at –0.83 and 1.52 V. The intensities of the first and second oxidation waves are almost half of other redox waves. The oxidation potentials of *meso*-dimesitylnorcorrole Ni(II) were 0.30 and 0.78 V. These results suggest that one-electron oxidation of **5** induces the formation of a mixed-valence dimer, which is attributable to the smaller steric hindrance around the *meso*-positions.[20] More clear splitting of the oxidation potentials was observed for norcorrole cyclophane **3**, whose first and second oxidation potentials are –0.13 and 0.26 V. This potential difference (0.39 V) lies between those of the covalently linked mixed-valence systems: bi(2,5-dimethoxy-4-methylphenyl) (0.29 V) and *N*,*N*,*N*′,*N*′-tetraanisyl-*p*-phenylenediamine (0.49 V).[21] The comproportionation constant of **5** was calculated to be 4×10^6.[22]

While no splitting was observed for porphyrin monomer **6**, porphyrin cyclophane **4** exhibited a small splitting between the first and second oxidations (0.25 V), which affords a comproportionation constant of 2×10^4. Importantly, this value is much smaller than that of norcorrole cyclophane **3** by about two orders of magnitude. These results clearly indicate that the interplanar interaction between two norcorroles in its mixed valence state is more effective than that between porphyrins.[23]

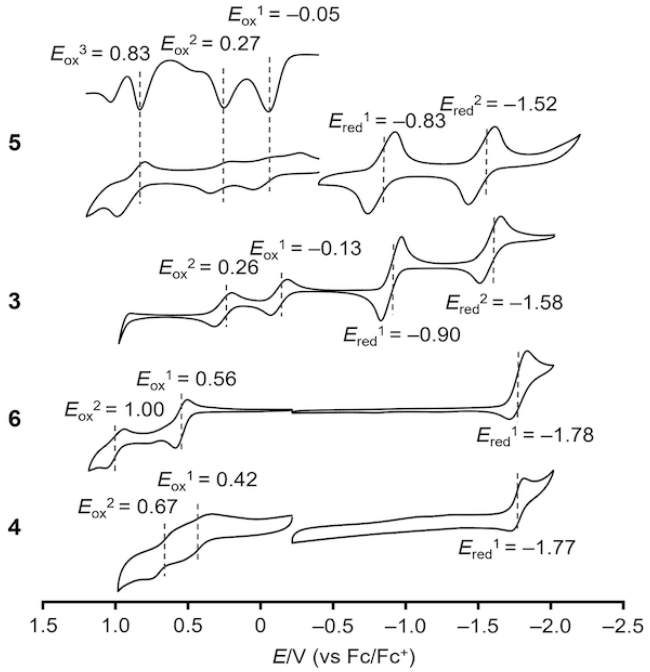

Figure 14. Cyclic voltammograms of **3**, **4**, **5**, and **6**. Solvent: CH_2Cl_2; supporting electrolyte: 0.1 M $[Bu_4N][PF_6]$; working electrode: Pt; counter electrode: Pt; reference electrode: $Ag/AgNO_3$; scan rate: 0.1 V s^{-1}.

CONCLUSIONS

We have synthesized two cyclophanes consisting of stacking Ni(II) norcorrole units and Ni(II) porphyrin units through ruthenium-catalyzed ring closing olefin metathesis of monomer precursors with terminal alkene moieties. The norcorrole cyclophane exhibits polymorphism affording three solid-state structures: aligned stacking (**A**), twisted stacking (**B**), and slip stacking (**C**). For these three structures, the aromaticity/antiaromaticity according to structural

and magnetic criteria was evaluated experimentally and theoretically. We found that 1) a small twist angle between two stacking norcorrole units and 2) a short displacement of two π-systems along the slipping axis result in distinct three-dimensional aromaticity, which is accomplished through effective overlap of molecular orbitals of the norcorrole macrocycles. In contrast, stacking of two aromatic porphyrins resulted in no significant change in their individual aromatic character. We also examined the structures and properties of norcorrole and porphyrin cyclophanes in solution. The detailed ^{1}H NMR analysis of these cyclophanes revealed the existence of an equilibrium between non-stacked and stacked states. The thermodynamic parameters of the stacking equilibrium elucidated inherently larger attractive interactions between two norcorrole macrocycles than those between two porphyrins, which has been corroborated by energy decomposition analysis. The present findings not only offer fundamental insights to understand the nature of stacked aromaticity, but also would lead to the design and creation of functional supramolecular architectures constructed by close π–π stacking of antiaromatic Ni(II) norcorrole units in the future.

ASSOCIATED CONTENT

Supporting Information

The Supporting Information is available free of charge on the ACS Publications website.
Experimental details and spectral data for all new compounds.
Crystallographic data (CIF files) for **A**, **B**, **C**, and **4**.

AUTHOR INFORMATION

Corresponding Author

hshino@chembio.nagoya-u.ac.jp; kowalct2@wwu.edu; heike.fliegl@kit.edu

Funding Sources

The authors declare the absence of any potentially competing financial interests.

ACKNOWLEDGMENT

This work was supported by JSPS KAKENHI grant JP20K21190 and JP20H05863. H.S. gratefully acknowledges the Ogasawara Foundation for the Promotion of Science and Engineering for financial support. S.U expresses his gratitude for a JSPS Research Fellowship for Young Scientists (JP20J11883). TK is a Cottrell Scholar of the Research Corporation for Science Advancement. We thank Dr. G. D. Pantos (University of Bath) for the detailed mass analysis of the norcorrole cyclophane.

REFERENCES

(1) (a) Desiraju, G. R.; Gavezzotti, A. From Molecular to Crystal Structure; Polynuclear Aromatic Hydrocarbons. *J. Chem. Soc., Chem. Commun.* **1989**, 621–623. (b) Thakuria, R.; Nath, N. K.; Saha, B. K. The Nature and Applications of π–π Interactions: A Perspective. *Cryst. Growth Des.* **2019**, *19*, 523–528. (c) Iwane, M.; Tada, T.; Osuga, T.; Murase, T.; Fujita, M.; Nishino, T.; Kiguchi, M.; Fujii, S. Controlling Stacking Order and Charge Transport in π-Stacks of Aromatic Molecules Based on Surface Assembly. *Chem. Commun.* **2018**, *54*, 12443–12446.

(2) (a) Burley, S. K.; Petsko, G. A. Aromatic-Aromatic Interaction: A Mechanism of Protein Structure Stabilization. *Science* **1985**, *229*, 23–28. (b) Hunter, C. A.; Singh, J.; Thornton, J. M. π–π Interactions: The Geometry and Energetics of Phenylalanine-Phenylalanine Interactions in Proteins. *J. Mol. Biol.* **1991**, *218*, 837–846. (c) Riley, K. E.; Hobza, P. On the Importance and Origin of Aromatic Interactions in Chemistry and Biodisciplines. *Acc. Chem. Res.* **2013**, *46*, 927–936. (d) Burley, S. K.; Petsko, G. A. Weakly Polar Interactions In Proteins. In *Advances in Protein Chemistry,* Anfinsen, C. B.; Edsall, J. T.; Richards, F. M.; Eisenberg, D. S. Eds.; Academic Press: 1988; Vol. 39, pp 125–189.

(3) (a) Hunter, C. A.; Sanders, J. K. M. The Nature of π–π Interactions. *J. Am. Chem. Soc.* **1990**, *112*, 5525–5534. (b) Cozzi, F.; Cinquini, M.; Annuziata, R.; Siegel, J. S. Dominance of Polar/π over Charge-Transfer Effects in Stacked Phenyl Interactions. *J. Am. Chem. Soc.* **1993**, *115*, 5330–5331. (c) Martinez, C. R.; Iverson, B. L. Rethinking the Term "Pi-Stacking." *Chem. Sci.* **2012**, *3*, 2191–2201.

(4) (a) Xiang, Q.; Guo, J.; Xu, J.; Ding, S.; Li, Z.; Li, G.; Phan, H.; Gu, Y.; Dang, Y.; Xu, Z.; Gong, Z.; Hu, W.; Zeng, Z.; Wu, J.; Sun, Z. Stable Olympicenyl Radicals and Their π-Dimers. *J. Am. Chem. Soc.* **2020**, *142*, 11022–11031. (b) Goto, K.; Kubo, T.; Yamamoto, K.; Nakasuji, K.; Sato, K.; Shiomi, D.; Takui, T.; Kubota, M.; Kobayashi, T.; Yakusi, K.; Ouyang, J. A Stable Neutral Hydrocarbon Radical: Synthesis, Crystal Structure, and Physical Properties of 2,5,8-Tri-*tert*-Butyl-Phenalenyl. *J. Am. Chem. Soc.* **1999**, *121*, 1619–1620.

(5) (a) Bröring, M.; Köhler, S.; Kleeberg, C. Norcorrole: Observation of the Smallest Porphyrin Variant with a N4 Core. *Angew. Chem. Int. Ed.* **2008**, *47*, 5658–5660. (b) Ito, T.; Hayashi, Y.; Shimizu, S.; Shin, J.-Y.; Kobayashi, N.; Shinokubo, H. Gram-Scale Synthesis of Nickel(II) Norcorrole: The Smallest Antiaromatic Porphyrinoid. *Angew. Chem. Int. Ed.* **2012**, *51*, 8542–8545.

(6) (a) Yoshida, T.; Sakamaki, D.; Seki, S.; Shinokubo, H. Enhancing the Low-Energy Absorption Band and Charge Mobility of Antiaromatic Ni(II) Norcorroles by Their Substituent Effects. *Chem. Commun.* **2017**, *53*, 1112–1115. (b) Yonezawa, T.; Shafie, S. A.; Hiroto, S.; Shinokubo, H. Shaping Antiaromatic π-Systems by Metalation: Synthesis of a Bowl-Shaped Antiaromatic Palladium Norcorrole. *Angew. Chem. Int. Ed.* **2017**, *56*, 11822–11825. (c) Fujii, S.; Marqués-González, S.; Shin, J.-Y.; Shinokubo, H.; Masuda, T.; Nishino, T.; Arasu, N. P.; Vázquez, H.; Kiguchi, M. Highly-Conducting Molecular Circuits Based on Antiaromaticity. *Nat. Commun.* **2017**, *8*, 15984. (d) Liu, B.; Li, X.; Stępień, M.; Chmielewski, P. J. Towards Norcorrin: Hydrogenation Chemistry and the Heterodimerization of Nickel(II) Norcorrole. *Chem. -Eur. J.* **2015**, *21*, 7790–7797. (e) Deng, Z.; Li, X.; Stępień, M.; Chmielewski, P. J. Nitration of Norcorrolatonickel(II): First Observation of a Diatropic Current in a System Comprising a Norcorrole Ring. *Chem. -Eur. J.* **2016**, *22*, 4231–4246. (f) Liu, B.; Yoshida, T.; Li, X.; Stępień, M.; Shinokubo, H.; Chmielewski, P. J. Reversible Carbon–Carbon Bond Breaking and Spin Equilibria in Bis(pyrimidinenorcorrole). *Angew. Chem. Int. Ed.* **2016**, *55*, 13142–13146. (g) Li, X.; Meng, Y.; Yi, P.; Stępień, M.; Chmielewski, P. J. Pyridine-Fused Bis(Norcorrole) through Hantzsch-Type Cyclization: Enhancement of Antiaromaticity by an Aromatic Bridge. *Angew. Chem. Int. Ed.* **2017**, *56*, 10810–10814.

(7) (a) Nozawa, R.; Tanaka, H.; Cha, W.-Y.; Hong, Y.; Hisaki, I.; Shimizu, S.; Shin, J.-Y.; Kowalczyk, T.; Irle, S.; Kim, D.; Shinokubo, H. Stacked Antiaromatic Porphyrins. *Nat. Commun.* **2016**, *7*, 13620. (b) Nozawa, R.; Kim, J.; Oh, J.; Lamping, A.; Wang, Y.; Shimizu, S.; Hisaki, I.; Kowalczyk, T.; Fliegl, H.; Kim, D.; Shinokubo, H. Three-Dimensional Aromaticity in an Antiaromatic Cyclophane. *Nat. Commun.* **2019**, *10*, 3576. (8) (a) Corminboeuf, C.; von Ragué Schleyer, P.; Warner, P. Are Antiaromatic Rings Stacked Face-to-Face Aromatic? *Org. Lett.* **2007**, *9*, 3263–3266. (b) Bean, D. E.; Fowler, P. W. Stacked-Ring Aromaticity: An Orbital Model. *Org. Lett.* **2008**, *10*, 5573–5576. (c) Kim, G.; Dutta, R.; Cha, W.-Y.; Hong, S.-J.; Oh, J.; Firmansyah, D.; Jo, H.; Ok, K. M.; Lee, C.-H.; Kim, D. Noncovalent Intermolecular Interaction in Cofacially Stacked 24π Antiaromatic Hexaphyrin Dimer. *Chem. - Eur. J.* **2020**, *26*, 16434–16440.

(9) For recent reviews, see: (a) Schrodi, Y.; Pederson, R. L. Evolution and Applications of Second-Generation Ruthenium Olefin Metathesis Catalysts. *Aldrichimica Acta* **2007**, *40*, 45–52. (b) Grubbs, R. H. Olefin-Metathesis Catalysts for the Preparation of Molecules and Materials. *Adv. Synth. Catal.* **2007**, *349*, 34–40. (c) Grubbs, R. H. Olefin metathesis. *Tetrahedron* **2004**, *60*, 7117–7140. (d) Trnka, T. M.; Grubbs, R. H. The Development of L_2X_2Ru=CHR Olefin Metathesis Catalysts: An Organometallic Success Story. *Acc. Chem. Res.* **2001**, *34*, 18–29. (e) Fürstner, A. Olefin Metathesis and Beyond. *Angew. Chem. Int. Ed.* **2000**, *39*, 3012–3043. (f) Schuster, M.;

Blechert, S. Olefin Metathesis in Organic Chemistry. *Angew. Chem. Int. Ed.* **1997**, *36*, 2036–2056.

(10) Krygowski, T. M.; Cyranski, M. K. Structural Aspects of Aromaticity. *Chem. Rev.* **2001**, *101*, 1385–1420.

(11) Chen, Z.; Wannere, C. S.; Corminboeuf, C.; Puchta, R.; Schleyer, P. von R. Nucleus-Independent Chemical Shifts (NICS) as an Aromaticity Criterion. *Chem. Rev.* **2005**, *105*, 3842–3888.

(12) (a) Jusélius, J.; Sundholm, D.; Gauss, J. Calculation of Current Densities Using Gauge-Including Atomic Orbitals. *J. Chem. Phys.* **2004**, *121*, 3952−3963. (b) Fliegl, H.; Taubert, S.; Lehtonen, O.; Sundholm, D. The Gauge Including Magnetically Induced Current Method. *Phys. Chem. Chem. Phys.* **2011**, *13*, 20500–20518. (c) Valiev, R. R.; Benkyi, I.; Konyshev, Y. V.; Fliegl, H.; Sundholm, D. Computational Studies of Aromatic and Photophysical Properties of Expanded Porphyrins. *J. Phys. Chem. A* **2018**, *122*, 4756–4767.

(13) Geuenich, D.; Hess, K.; Köhler, F.; Herges, R. Anisotropy of the Induced Current Density (ACID), a General Method to Quantify and Visualize Electronic Delocalization. *Chem. Rev.* **2005**, *105*, 3758–3772.

(14) (a) Valiev, R. R.; Fliegl, H.; Sundholm, D. Closed-Shell Paramagnetic Porphyrinoids. *Chem. Commun.* **2017**, *53*, 9866–9869. (b) Lehtola, S.; Dimitrova, M.; Fliegl, H.; Sundholm, D. Benchmarking Magnetizabilities with Recent Density Functionals. *J. Chem. Theory Comput.* **2021**, *17*, 1457–1468.

(15) Brown, J. S. QC_Tools or CATNIP – Charge Transfer Integral Package. https://github.com/JoshuaSBrown/QC_Tools (accessed 2021-06-10).

(16) Stępień, M.; Latos-Grażyński, L.; Sprutta, N.; Chwalisz, P.; Szterenberg, L. Expanded Porphyrin with a Split Personality: A Hückel–Möbius Aromaticity Switch. *Angew. Chem. Int. Ed.* **2007**, *46*, 7869–7873.

(17) (a) Crabtree, R. Iridium Compounds in Catalysis. *Acc. Chem. Res.* **1979**, *12*, 331–337. (b) Weck, M.; Mohr, B.; Sauvage, J.-P.; Grubbs, R. H. Synthesis of Catenane Structures via Ring-Closing Metathesis. *J. Org. Chem.* **1999**, *64*, 5463–5471.

(18) Leighton, P.; Cowan, J. A.; Abraham, R. J.; Sanders, J. K. M. Geometry of Porphyrin–Porphyrin Interactions. *J. Org. Chem.* **1988**, *53*, 733–740.

(19) Mao, Y.; Horn, P. R.; Head-Gordon, M. Energy Decomposition Analysis in an Adiabatic Picture. *Phys. Chem. Chem. Phys.* **2017**, *19*, 5944–5958.

(20) (a) Sun, D.-L.; Rosokha, S. V.; Lindeman, S. V.; Kochi, J. K. Intervalence (Charge-Resonance) Transitions in Organic Mixed-Valence Systems. Through-Space versus Through-Bond Electron Transfer between Bridged Aromatic (Redox) Centers. *J. Am. Chem. Soc.* **2003**, *125*, 15950–15963. (b) Nakamura, K.; Okada, Y.; Shirahata, T.; Misaki, Y. Cyclic TTF Tetramer Linked by Methylenedithio Spacers. *Chem. Lett.* **2014**, *43*, 708–710.

(21) (a) Lindeman, S. V.; Rosokha, S. V.; Sun, D.; Kochi, J. K. X-Ray Structure Analysis and the Intervalent Electron Transfer in Organic Mixed-Valence Crystals with Bridged Aromatic Cation Radicals. *J. Am. Chem. Soc.* **2002**, *124*, 843–855. (b) Lambert, C.; Nöll, G. The Class II/III Transition in Triarylamine Redox Systems. *J. Am. Chem. Soc.* **1999**, *121*, 8434–8442.

(22) Richardson, D. E.; Taube, Henry. Determination of E_2^0–E_1^0 in Multistep Charge Transfer by Stationary-Electrode Pulse and Cyclic Voltammetry: Application to Binuclear Ruthenium Ammines. *Inorg. Chem.* **1981**, *20*, 1278–1285.

(23) Robin, M. B.; Day, P. Mixed Valence Chemistry-A Survey and Classification. In *Advances in Inorganic Chemistry and Radiochemistry*; Emeléus, H. J., Sharpe, A. G., Eds.; Academic Press: 1968; Vol. 10, pp 247–422.

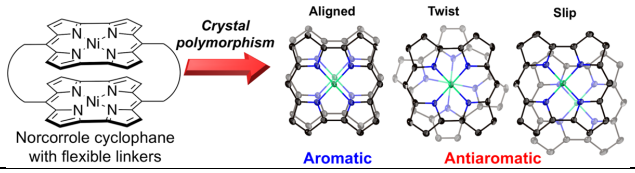
Crystal
polymorphism
Aligned
Twist
Slip
Norcorrole cyclophane
with flexible linkers
Aromatic
Antiaromatic